Supporting information

Regulating Memristor Performance of Organic-Inorganic Hybrid Polyoxometalates via Counter Cations

Hui-Xue Lei, Ze-Xun Zhang, Xin-Xiong Li, Qiao-Huang Wei,* Hao-Hong Li,* and Shou-Tian Zheng*

1 Section S1 Experimental Procedures

Table S1. Crystal data and structure refinement parameters for compound **1** and **2.**

compound	**1**	**2**
Empirical formula	$C_{90}H_{80}CuIMnMo_6N_2O_{24}P_3$	$C_{68}H_{80}CuIMnMo_6N_2O_{24}P_2$
Formula weight	2487.62	2781.15
Crystal system	triclinic	triclinic
Space group	*P-1*	*P-1*
a (Å)	12.183(2)	16.838(2)
b (Å)	19.984(4)	17.871(2)
c (Å)	20.262(4)	20.708(3)
α (°)	83.979(3)	91.900(2)
β (°)	74.039(3)	100.406(2)
γ (°)	75.983(3)	107.973(2)
V (Å^{-3})	4597.7(14)	5803.4(12)
Z	2	2
ρ_{calc} (g cm^{-3})	1.797	1.591
μ (mm^{-1})	1.612	1.277
F (000)	2460.0	2794.0
Temperature/K	170.0	170.0
Reflections collected	47144	50078
Size (mm)	0.1 × 0.1 × 0.08	0.12 × 0.1 × 0.05
Independent reflections	15645 [R_{int}= 0.0964, R_{sigma}= 0.1167]	19877 [R_{int}= 0.0269, R_{sigma}= 0.0371]
Data/restraints/parameters	15645/0/1156	19877/161/946
Goodness-of-fit on F^2	1.038	1.030
Final R indexes [I>=2σ (I)]	R_1 = 0.0796, wR_2 = 0.2219	R_1 = 0.0523, wR_2 = 0.1597
Final R indexes [all data]	R_1 = 0.1499, wR_2 = 0.2838	R_1 = 0.0625, wR_2 = 0.1745

$R_1 = \sum||F_o| - |F_c||/\sum|F_o|$. $wR_2 = [\sum w(F_o^2 - F_c^2)^2/\sum w(F_o^2)^2]^{1/2}$; $w = 1/[\sigma^2(F_o^2) + (xP)^2 + yP]$, $P = (F_o^2 + 2F_c^2)/3$

Table S2. The bond valence sum calculations of the Mo, Mn and Cu atoms in compounds **1** and **2.**

Compound **1**			Compound **2**		
Atoms code	Bond Value	Valence state	Atoms code	Bond Value	Valence state
Mo1	6.082	+6	Mo1	5.997	+6
Mo2	6.157	+6	Mo2	5.948	+6
Mo3	6.030	+6	Mo3	5.983	+6
Mo4	6.065	+6	Mo4	6.070	+6
Mo5	6.198	+6	Mo5	6.046	+6
Mo6	6.006	+6	Mo6	5.948	+6
Mn1	3.399	+3	Mn1	3.386	+3
Mn2	3.419	+3	Mn2	3.446	+3
Cu1	0.908	+1	Cu1	0.903	+1

Table S3. RS parameters of memory devices in this work.

device	RS performance type	V_{set}/V_{reset}	$I_{on/off}$
ITO/CuI/Ag	silent	-	-
ITO/$MnMo_6O_{18}L_2$/Ag	flash	1.38 V/-4.19 V	4.11
ITO/Ph_4PBr/Ag	flash	2.33 V/-7.90 V	88.99
ITO/$C_{24}H_{28}PBr$/Ag	flash	1.35 V/-4.12 V	1.45
ITO/**1**/Ag	worm	1.12 V/-	2.88×10^4
ITO/**2**/Ag	worm	0.99 V/-	1.01×10^3
ITO/**1**/Ag at 200 ºC	worm	0.67 V/-	1.78×10^3
ITO/**2**/Ag at 200 ºC	worm	0.80 V/-	4.65×10^2

Table S4. The comparison with relative POM-based memristors.

device	RS performance type	V_{set}/V_{reset}	$I_{on/off}$	tolerant temperature	Ref.
ITO/$Na_{10}(H_2O)_{36}[Co_2(phen)_2$ (4,4′ bipy)$(Nb_6O_{19})_2]\cdot 19H_2O$/Ag	flash	1.12 V/−7 V	1.18×10^3	70 °C	[1]
ITO/ $Na_6V_{10}O_{28}$/Cr/Au	flash	1.2 V/0.8 V	25	/	[2]
ITO/{$[Co_2(bpdo)_4(H_2O)_6]$ (α-$GeW_{12}O_{40}$)}$\cdot 4(H_2O)\}_n$/Ag	flash	1.77 V/−3.42 V	1.0×10^2	150 °C	[3]
ITO/$H_4[Na(H_2O)_5]_2$ $[Co^{II}(en)_3]2\{[Co^{III}(en)]_2$ $(Ta_6O_{19})_2\}22H_2O$ /Ag	flash	3.79 V/−7.64 V	1.43×10^3	/	[4]
ITO/$[Co(H_2O)_6]_2[Co_3(bpdo)_4(H_2O)_{10}][Co_4(H_2O)_2$(B-a $PW_9O_{34})_2]\cdot 2$ bpdo$\cdot 14H_2O$ /A	flash	-0.63 V/0.75 V	55.5	270 °C	[5]
ITO/$(MV)_2[Cu_2I_3]$(Mn $Mo_6O_{18}L_2)\cdot 4CH_3CN$ /Ag	flash	0.97 V/-3.49 V	2.32×10^2	240 °C	[6]
ITO/$H_3PW_{12}O_{40}$@PMMA/Au	flash	1.2 V/-1.71 V	6×10^2	/	[7]
FTO/ $[Ni(en)_3]_2[\beta - V_8^{IV}V_2^{V}B_{28}O_{56}(OH)_{18}$ /Ag	worm	0.82 V	6.67×10^3	/	[8]
FTO/$(H_2$1,3$dap)_6[V_8^{IV}V_2^{V}B_{26}O_{64}$ $(OH)_4$(1,3$dap)_2\cdot$(1,3$dap)$]2$\cdot H_2O_/$ Ag	worm	0.79 V	1.07×10^4	/	

ITO/**1**/Ag	worm	0.99 V	2.88×10^4	200 °C	This work
ITO/**2**/Ag	worm	1.12 V	1.01×10^3	200 °C	This work

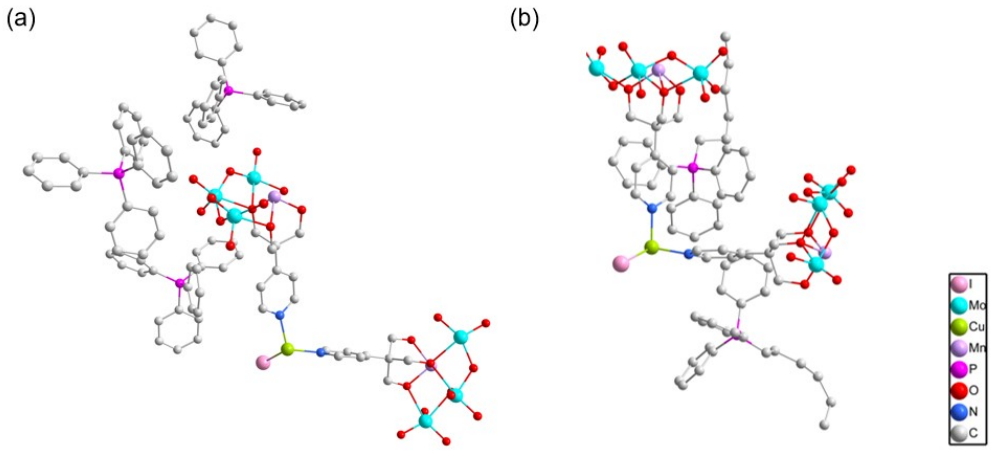

Fig. S1. Asymmetric units of compound **1** (a) and compound **2** (b)**.**

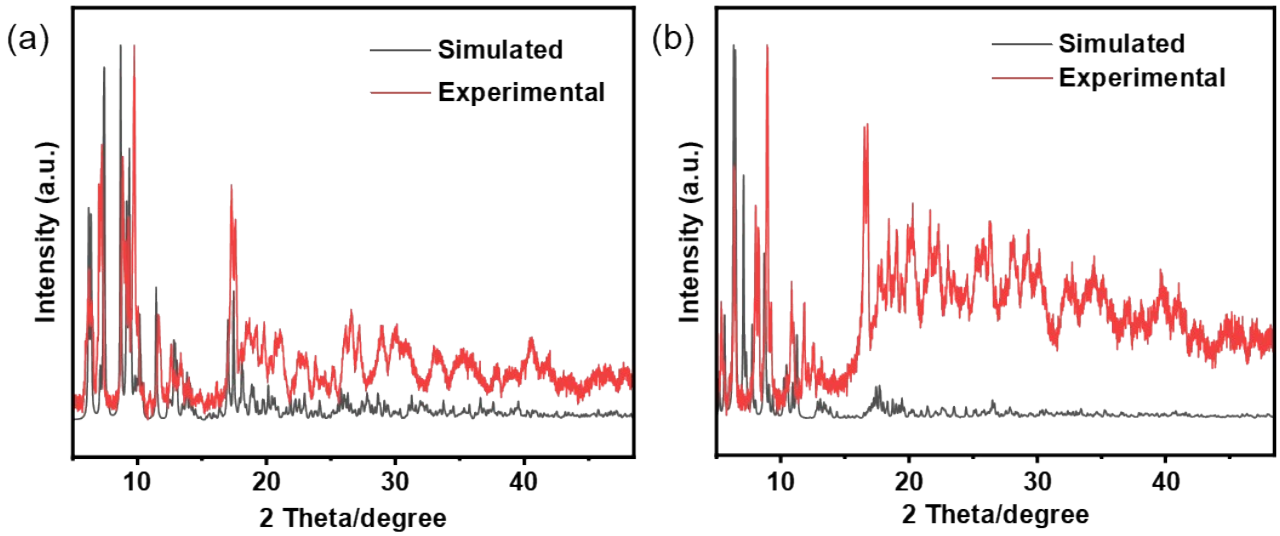

Fig. S2. The simulated and experimental PXRD patterns of compound **1**(a) and compound **2** (b)**.**

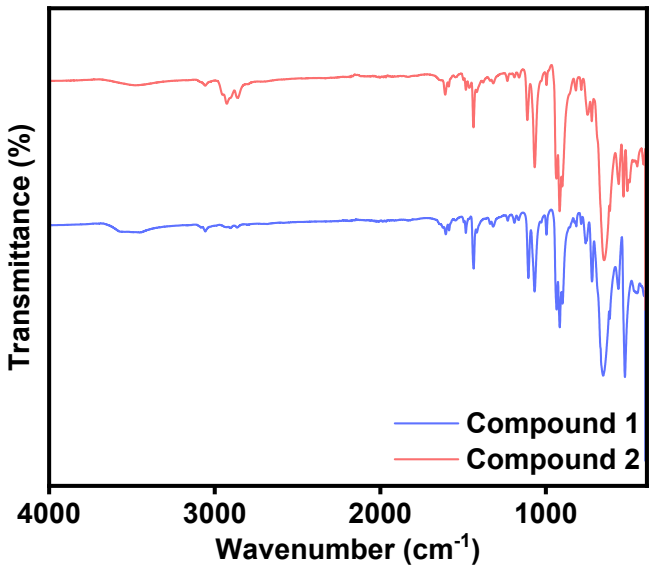

Fig. S3. IR spectra of compound **1** and compound **2.**

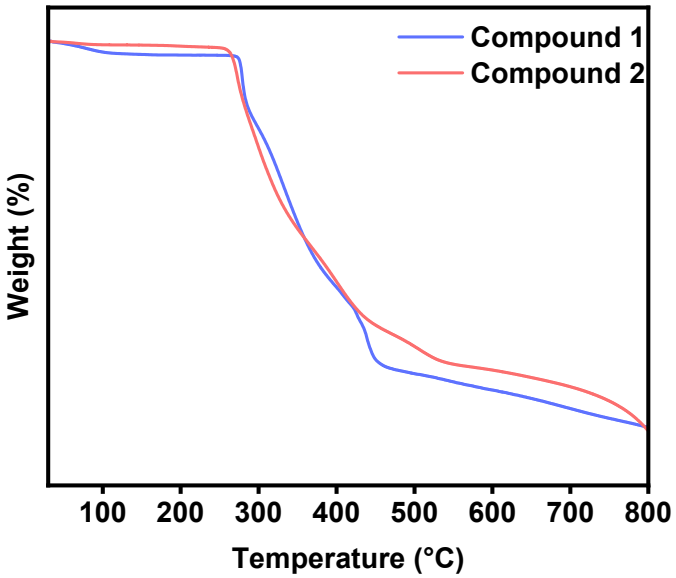

Fig. S4. TG curves of compound **1** and compound **2**.

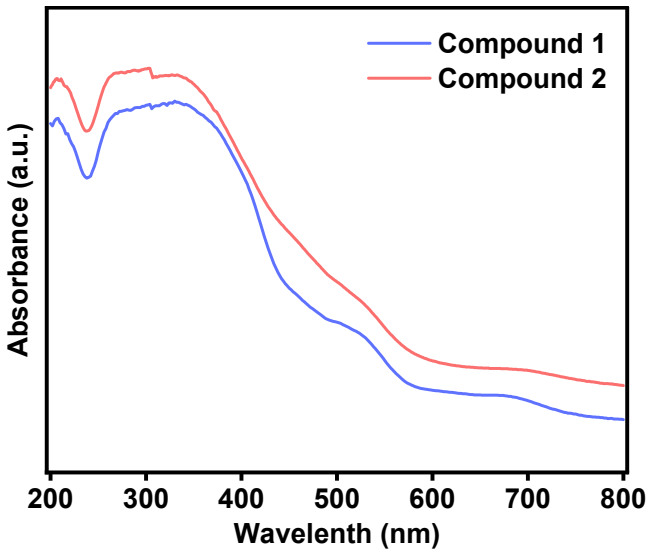

Fig. S5. UV-Vis absorption spectra of compound **1** and compound **2.**

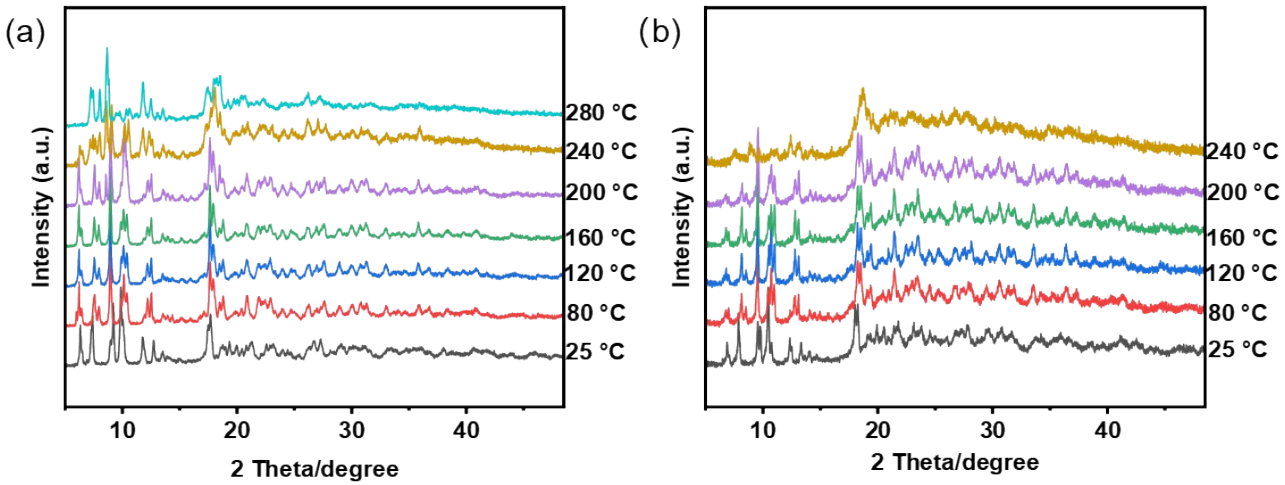

Fig. S6. Temperature-dependent PXRD patterns of compound **1** (a) and compound **2** (b).

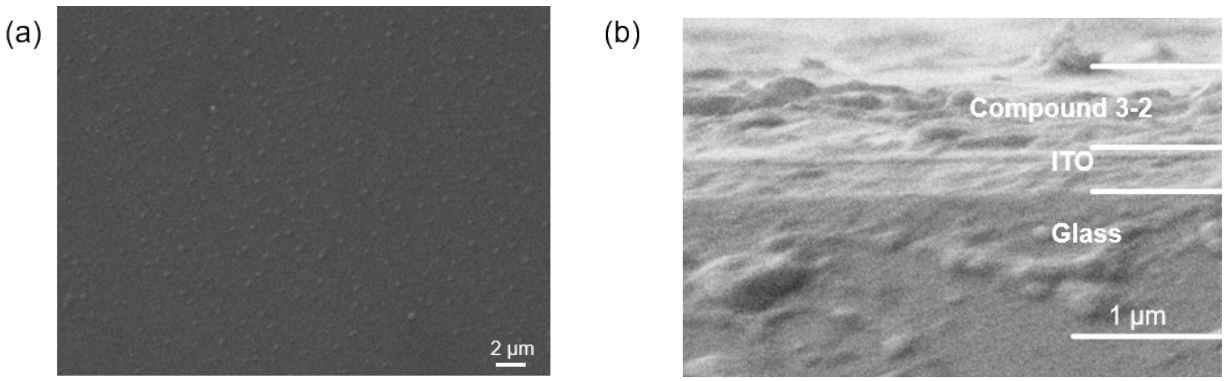

Fig. S7. (a) The surface SEM image of ITO/**2**/Ag memory device and (b) the cross-sectional SEM images of the ITO/**2**/Ag memory device.

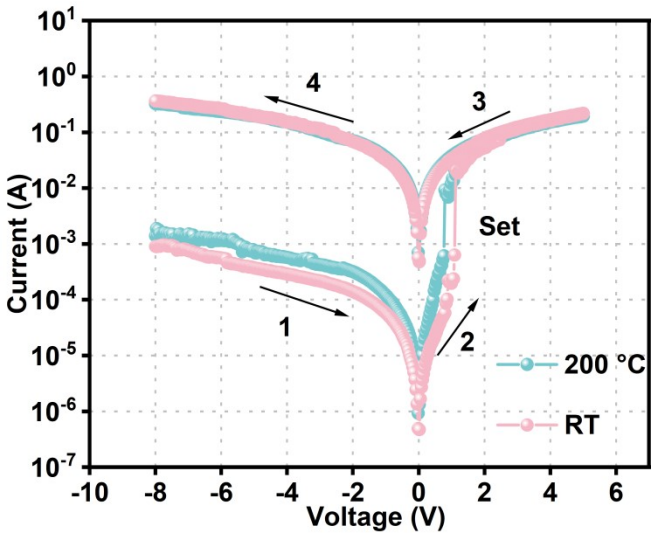

Fig. S8. *I-V* curves of ITO/**2**/Ag at different temperatures.

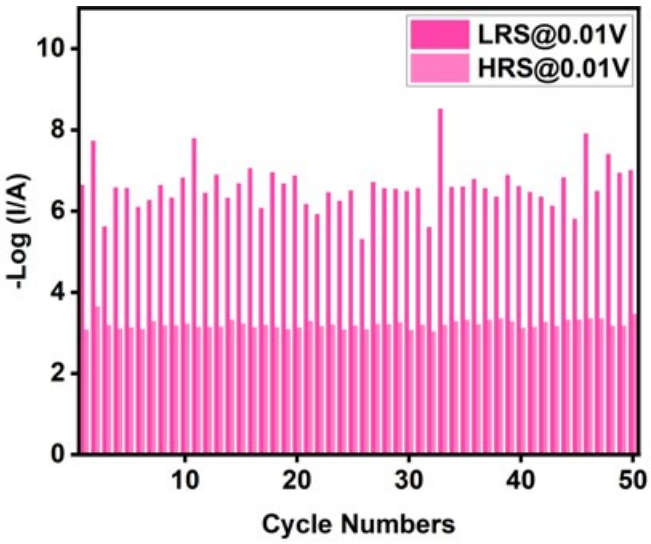

Fig. S9. Cyclic tolerance diagram for ITO/**2**/Ag at RT.

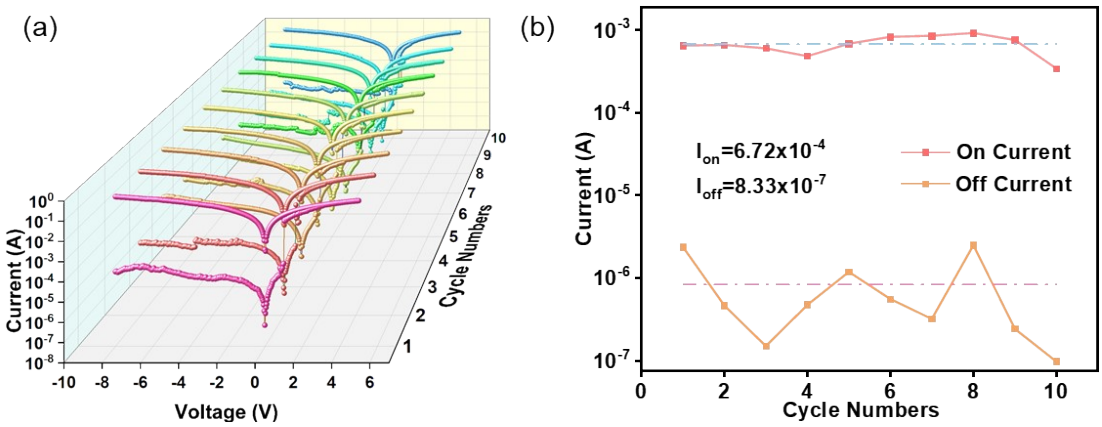

Fig. S10. For ITO/**2**/Ag at RT. (a) Ten cycles *I-V* curves. (b) The current changes of HRS and LRS following ten cycles.

Fig. S11. Cyclic tolerance diagram for ITO/**2**/Ag at 200 °C.

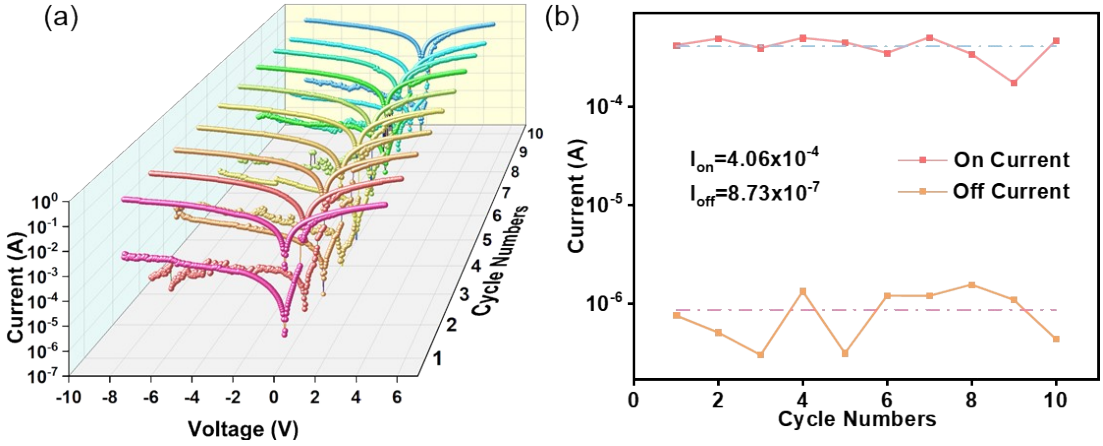

Fig. S12. For ITO/**2**/Ag at 200 °C. (a) Ten cycles *I-V* curves. (b) The current changes of HRS and LRS following ten cycles.

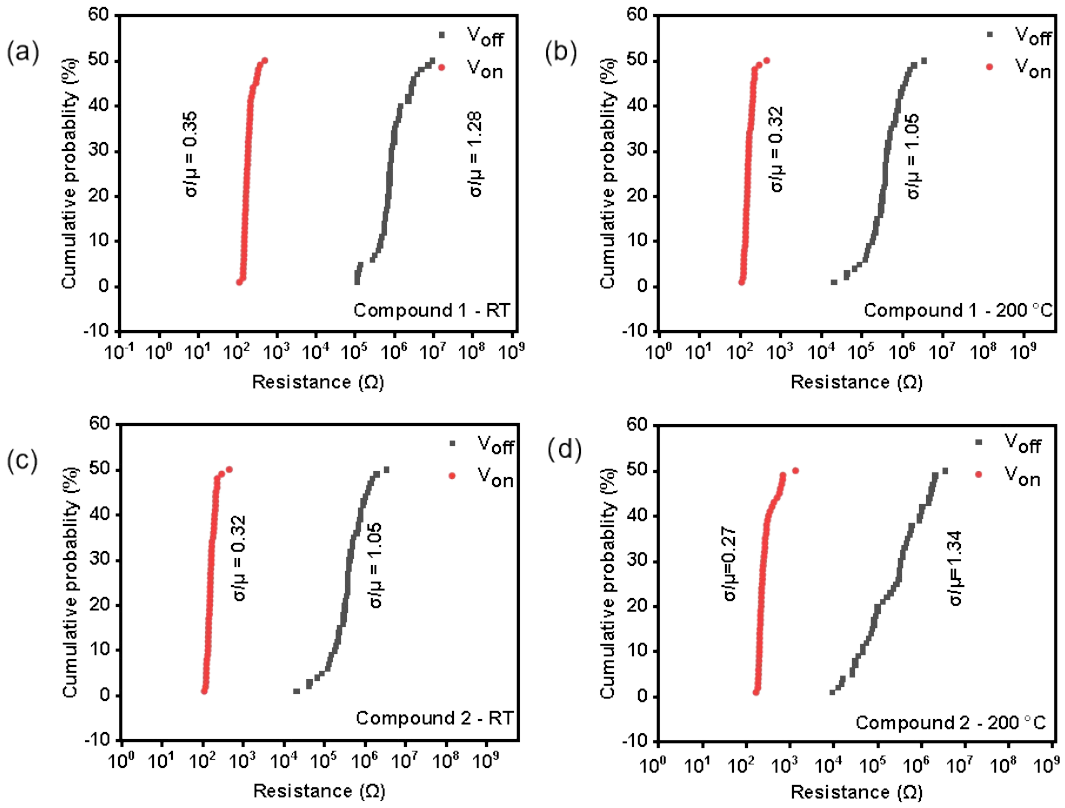

Fig. S13. CP of OFF and ON current distributions (a) ITO/**1**/Ag at RT; (b) ITO/**1**/Ag at 200 °C; (c) ITO/**2**/Ag at RT; (d) ITO/**2**/Ag at 200 °C.

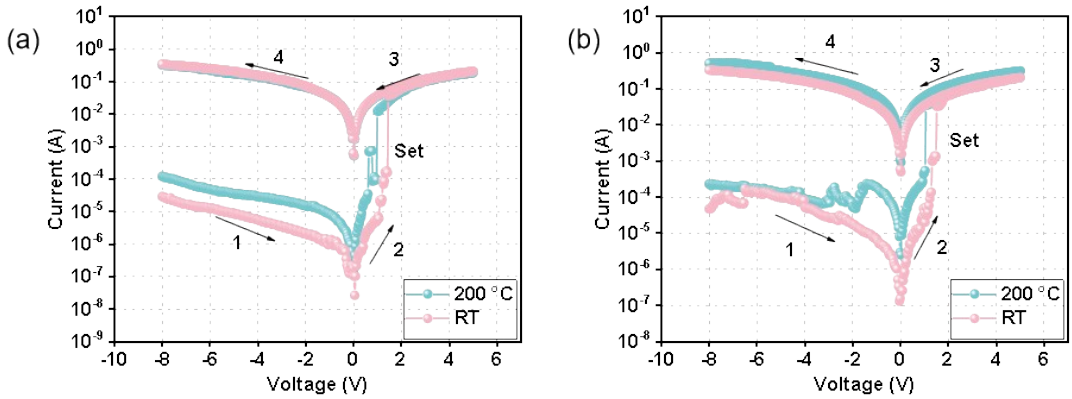

Fig. S14. After 1 year (a) *I-V* curves of ITO/**1**/Ag at different temperature; (b) *I-V* curves of ITO/**2**/Ag at different temperature.

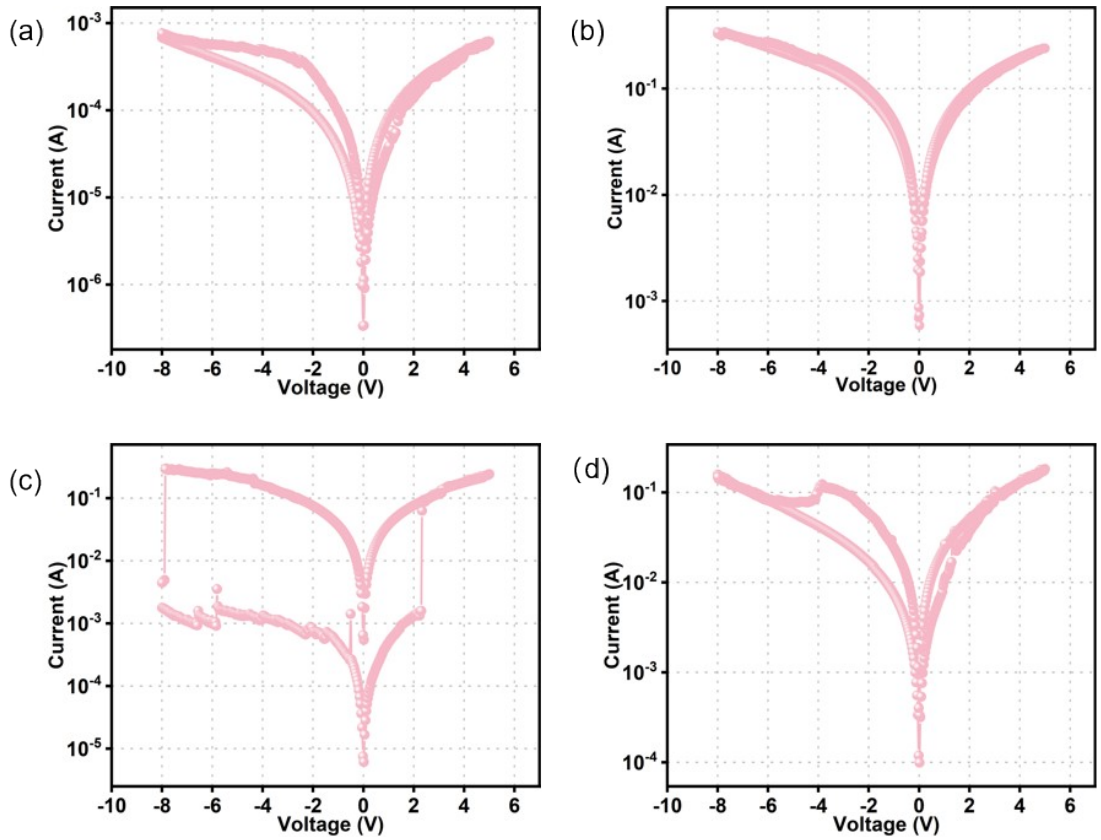

Fig. S15. *I-V* curves (a) ITO/$(TBA)_3[MnMo_6O_{18}L_2]\cdot 2CH_3CN$ /Ag; (b) ITO/CuI/Ag; (c) ITO/Ph_4PBr/Ag; (d) ITO/ n-HTPPBr/Ag.

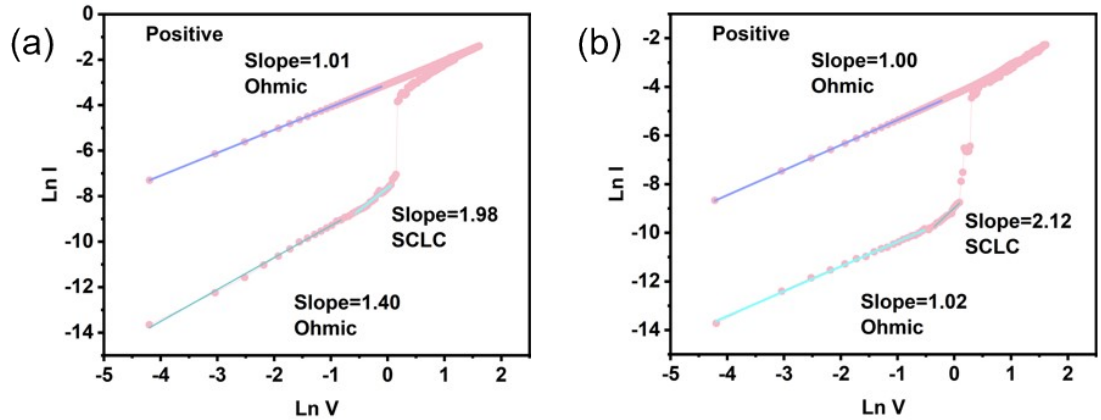

Fig. S16. Ln–ln plots on the *I–V* curves of the ITO/**2**/Ag device (a) in the Set process at RT; (b) in the Set process at 200 °C.

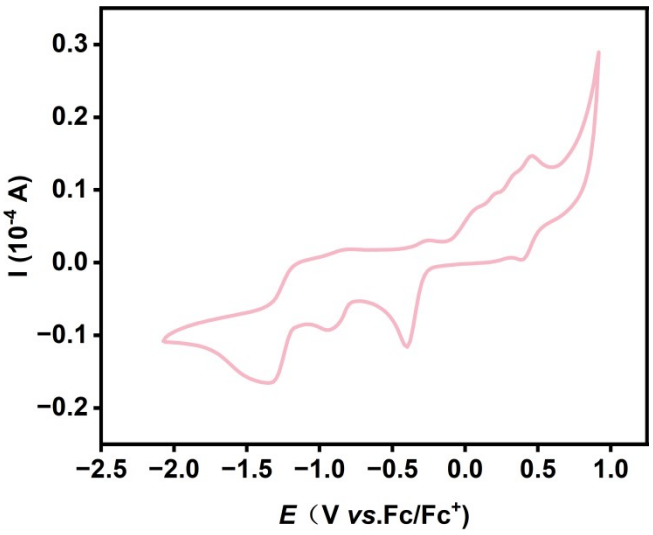

Fig. S17. CV curves of **2**.

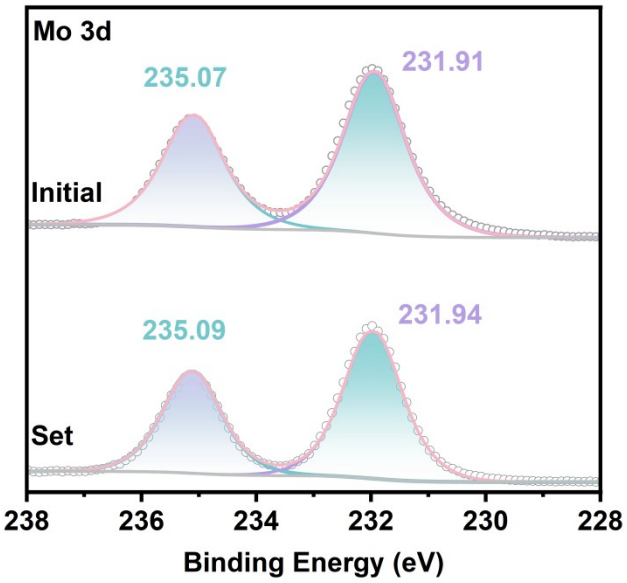

Fig. S18. XPS spectra of **1** Mo 3d.

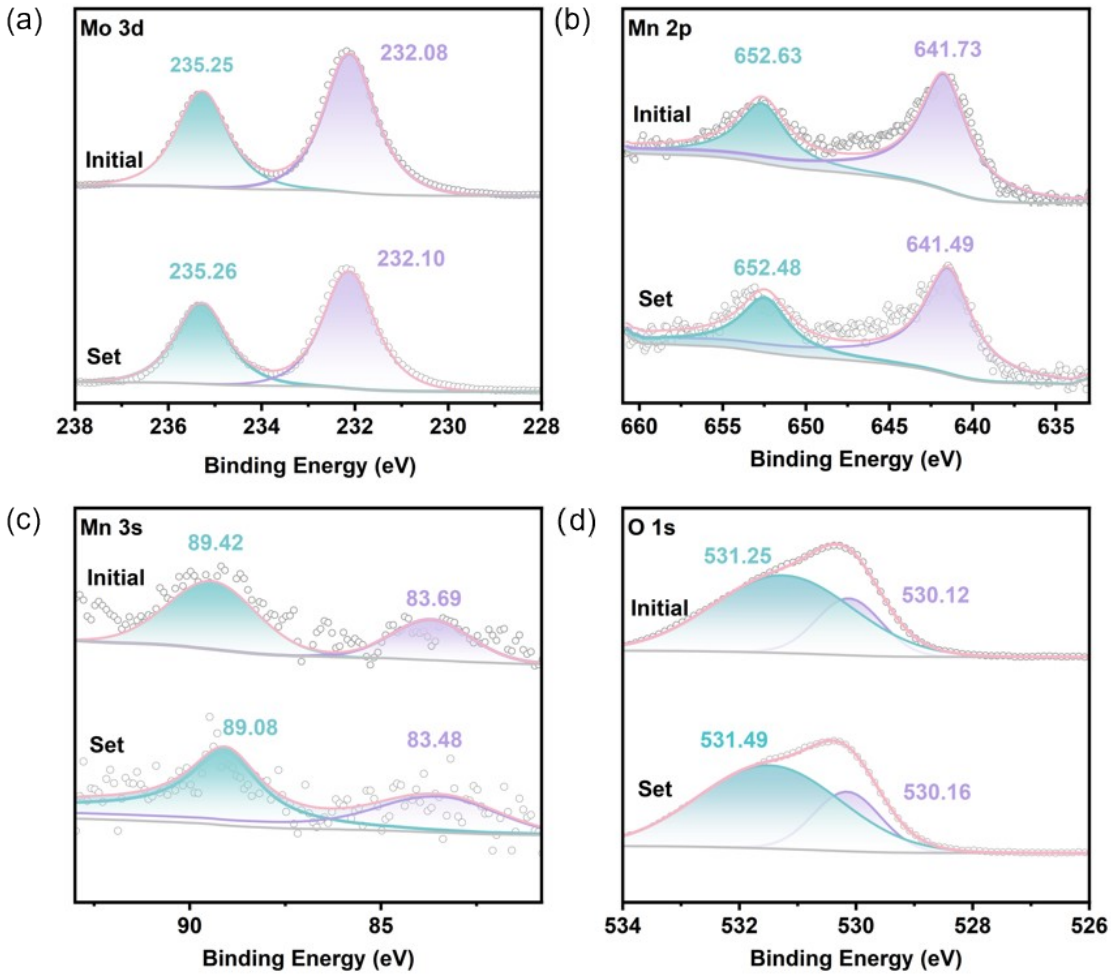

Fig. S19. XPS spectra of **2**: (a) Mo 3d; (b) Mn 2p; (c) Mn 3s; (d) O 1s.

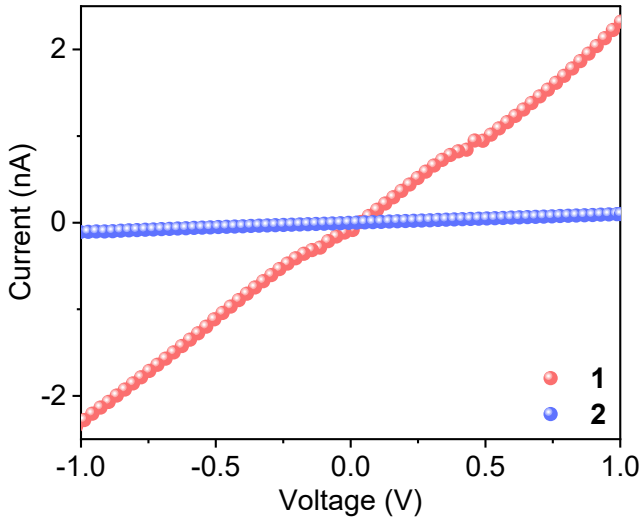

Fig. S20. *I-V* curves of pellet sample **1** and **2**.

References:

1. Y.-J. Wang, N. Shi, C. Sun, Y.-Q. Sun and S.-T. Zheng, *Inorg. Chem.*, 2023, **62**, 10675-10683.
2. S. N. S, N. Basu, M. Cahay, S. M. N, S. S. Mal and P. P. Das, *Phys. Status Solidi A.*, 2020, **217**, 2000306.
3. B. Chen, Y.-R. Huang, K.-Y. Song, X.-L. Lin, H.-H. Li and Z.-R. Chen, *Chem. Mater*, 2021, **33**, 2178-2186.
4. Y.-F. Cao, Y.-J. Lin, X.-X. Li, Y.-Q. Sun and S.-T. Zheng, *CrystEngComm*, 2024, **26**, 3527-3534.
5. Y. R. Huang, X. L. Lin, B. Chen, H. D. Zheng, Z. R. Chen, H. H. Li and S. T. Zheng, *Angew. Chem. Int. Ed.*, 2021, **60**, 16911-16916.
6. H.-B. Chen, M.-Y. He, T. Li, C.-C. Deng, H.-P. Xiao, M.-Q. Qi, X.-J. Kong, H.-H. Li, X.-X. Li and S.-T. Zheng, *J. Mater. Chem. C*, 2024, **12**, 13555-13561.
7. X. Chen, P. Huang, X. Zhu, S. Zhuang, H. Zhu, J. Fu, A. S. Nissimagoudar, W. Li, X. Zhang, L. Zhou, Y. Wang, Z. Lv, Y. Zhou and S.-T. Han, *Nanoscale Horiz*, 2019, **4**, 697-704.
8. M.-Z. Meng, Y.-Q. Gao, Y.-P. Chen, H.-H. Li and X.-H. Huang, *Inorg. Chem. Front*, 2025, **12**, 3186-3195.